



# A DFT study on the adsorption of nucleobases with Au<sub>20</sub>

Shengqiang Zhou<sup>1</sup> · Xiyuan Sun<sup>1</sup> · Gang Jiang<sup>2</sup>

Received: 3 August 2020 / Accepted: 22 November 2020 / Published online: 7 January 2021  
© Springer-Verlag GmbH Germany, part of Springer Nature 2021

## Abstract

The interactions of nucleobase with Au<sub>20</sub> cluster were studied utilizing density functional theory (DFT). We find that the nucleobases were attached with Au<sub>20</sub> through Au–N or Au–O bonds. The orders of calculated adsorption energy are cytosine > adenine > guanine > thymine. The maximum adsorption energy is –0.787 eV which belongs to the adsorption of cytosine on Au<sub>20</sub> cluster. Our calculations show that the HOMO-LUMO gaps of Au<sub>20</sub> are significantly decreased by the nucleobase adsorption, suggesting the potential detection for nucleobases. The interactions between Au<sub>20</sub> and nucleobases are revealed through the QTAIM analysis. The NBO analysis was investigated for the electron transfer of donor-acceptor of all types of complexes. The IR and UV-vis spectra were simulated for the further identification in the experiment.

**Keywords** Au<sub>20</sub> cluster · Nucleobase · Adsorption · DFT · QTAIM

## Introduction

The nucleobases play the most important role in the formation of biological systems and sever as the cornerstone of DNA and RNA. Therefore, how to use the interaction with the surface of the nucleobases to sequence DNA molecules is considered in the development of biological technologies [1]. DNA sequence detection is of great value in the diagnosis of genetic diseases, military counter-terrorism, and environmental monitoring. In recent years, electrochemical DNA biosensor has become a very active research field for DNA sequence detection due to its characteristics of sensitivity, capacity, low cost, and low energy consumption [2]. Many of these studies have been based on the interaction between DNA/RNA and carbon nanotubes instead of noble metal [3–5].

In the last decade, the scale of the human application of gold has become more elaborate. At the scale of clusters, gold clusters exhibit many special physical and chemical properties [6–8]. Of the dozens of clusters, Au<sub>20</sub> is a unique molecular cluster with a Td symmetry pyramid structure [9]. The magic configuration

which makes all atoms is on the surface of the cluster; that is to say, there are three types of adsorption sites. Hence, the ligand-protected Au<sub>20</sub> has attracted interest in coordination chemistry [10, 11]. The Au<sub>20</sub> possesses excellent stability and chemical inertness due to its large HOMO/LUMO gap which is greater than C<sub>60</sub> [12]. It has important applications with hypotonicity and high quantum yield in vivo, for instance, applying in cancer detection, drug delivery, cell labeling, biosensor, and cell transfection [13–17]. It is found that Au<sub>20</sub> is easily covalently bound to S atom; this demonstrates that Au<sub>20</sub> can specifically bind to other adaptive amino acids by binding to cysteine as a mediator. Therefore, Au<sub>20</sub> is a very promising candidate as a fluorescent probe and biosensor.

In this study, we have studied the interaction of nucleobases, adenine (A), cytosine (C), guanine (G), and thymine (T) on the Au<sub>20</sub> cluster by using density functional theory (DFT). The adsorption energies, HOMO-LUMO gaps, and the electron transfers were calculated. Quantum theory of atoms in molecules (QTAIM) and natural bond orbital (NBO) were used to reveal the interaction characteristics. This research may provide new insights into gold nanoclusters as biosensors.

✉ Xiyuan Sun  
sunxy@sicau.edu.cn

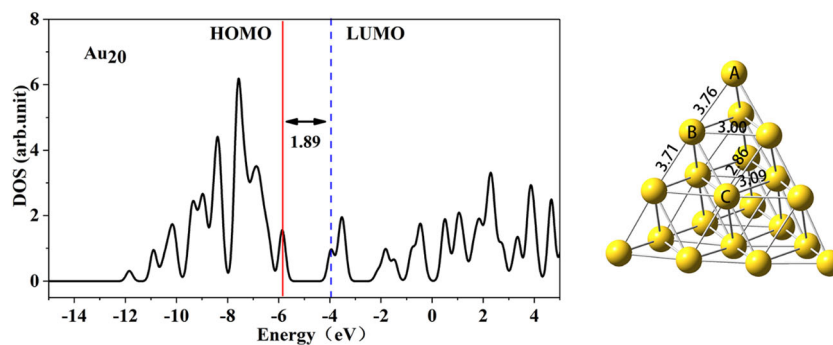
<sup>1</sup> College of Science, Sichuan Agricultural University, Ya'an 625014, People's Republic of China

<sup>2</sup> Institute of atomic and molecular physics, Sichuan University, Chengdu 610065, China

## Computational details

All of our quantum chemical calculations were performed with the Gaussian 09 [18] in the framework of the generalized

**Fig. 1** Geometrical parameters of Au<sub>20</sub> and its calculated density of state (DOS) plot; distances are in Å



gradient approximation (GGA) with PBE functional [19, 20]. The valence electrons of nucleobases and Au<sub>20</sub> are described with the 6-311++G (d, p) and LANL2DZ basis sets, respectively. We defined adsorption energy ( $E_{ad}$ ) of complexes in the usual way as follows:

$$E_{ad} = E_{\text{complex}(A,B,C,D)} - E_{\text{isolate}(Au_{20})} - E_{\text{nucleobase}(A,C,G,T)} \quad (1)$$

where the  $E_{\text{complex}}$ ,  $E_{\text{isolate}}$ , and  $E_{\text{nucleobase}}$  are the energies of the Au<sub>20</sub>/nucleobase complexes, the isolated cluster, and nucleobases, respectively. Furthermore, the energy gap  $E_g$  is

**Fig. 2** The energetically favorable configurations of Au<sub>20</sub>/nucleobase complexes

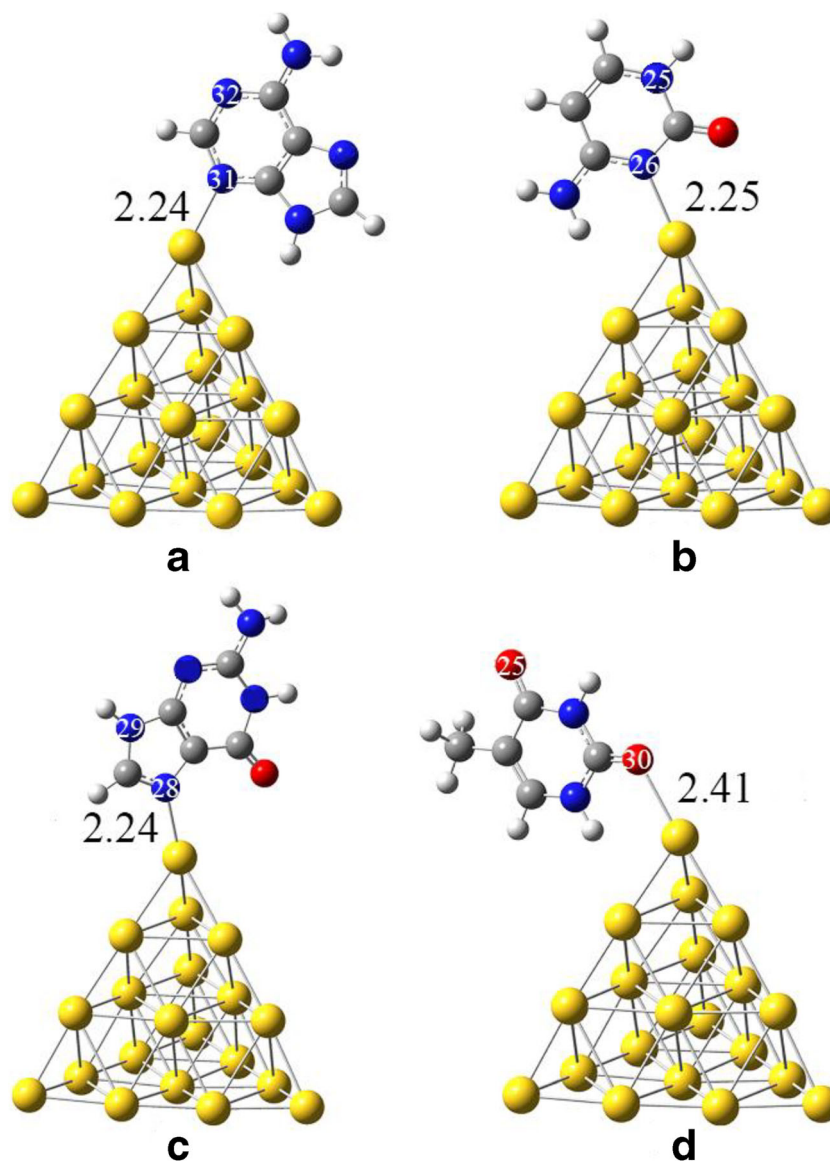


**Table 1** HOMO energies ( $E_{\text{HOMO}}$ ), LUMO energies ( $E_{\text{LUMO}}$ ), HOMO-LUMO energy gap ( $E_g$ ), adsorption energy ( $E_{\text{ad}}$ ) with basis set superposition errors, adsorption energy in aqueous solution  $E(S)_{\text{ad}}$ , and the gap change ( $\Delta E_g$ )

complex	$E_{\text{HOMO}}$	$E_{\text{LUMO}}$	$E_g$	$E_{\text{ad}}$	$E(S)_{\text{ad}}$	$\Delta E_g$ (%)
Au <sub>20</sub>	-5.842	-3.953	1.889			–
A	-5.361	-3.717	1.644	-0.690	-0.472	12.97
B	-5.212	-3.564	1.648	-0.787	-0.530	12.81
C	-5.045	-3.370	1.675	-0.688	-0.390	11.33
D	-5.658	-3.902	1.756	-0.328	-0.254	7.00

(A, B, C, and D are Au<sub>20</sub>/adenine, Au<sub>20</sub>/cytosine, Au<sub>20</sub>/guanine, and Au<sub>20</sub>/thymine, respectively)

defined as follows:

$$E_g = E_{\text{LUMO}} - E_{\text{HOMO}} \quad (2)$$

In this equation,  $E_{\text{HOMO}}$  is the energy of the highest occupied molecular orbital (HOMO) and  $E_{\text{LUMO}}$  is the energy of the lowest unoccupied molecular orbital (LUMO). The change of energy gap ( $\Delta E_g$ ) is an important parameter when we estimate the properties of the sensor:  $\Delta E_g$  is defined by:

$$\Delta E_g = \frac{|E_{\text{complex}} - E_{\text{isolate}}|}{E_{\text{isolate}}} \times 100\% \quad (3)$$

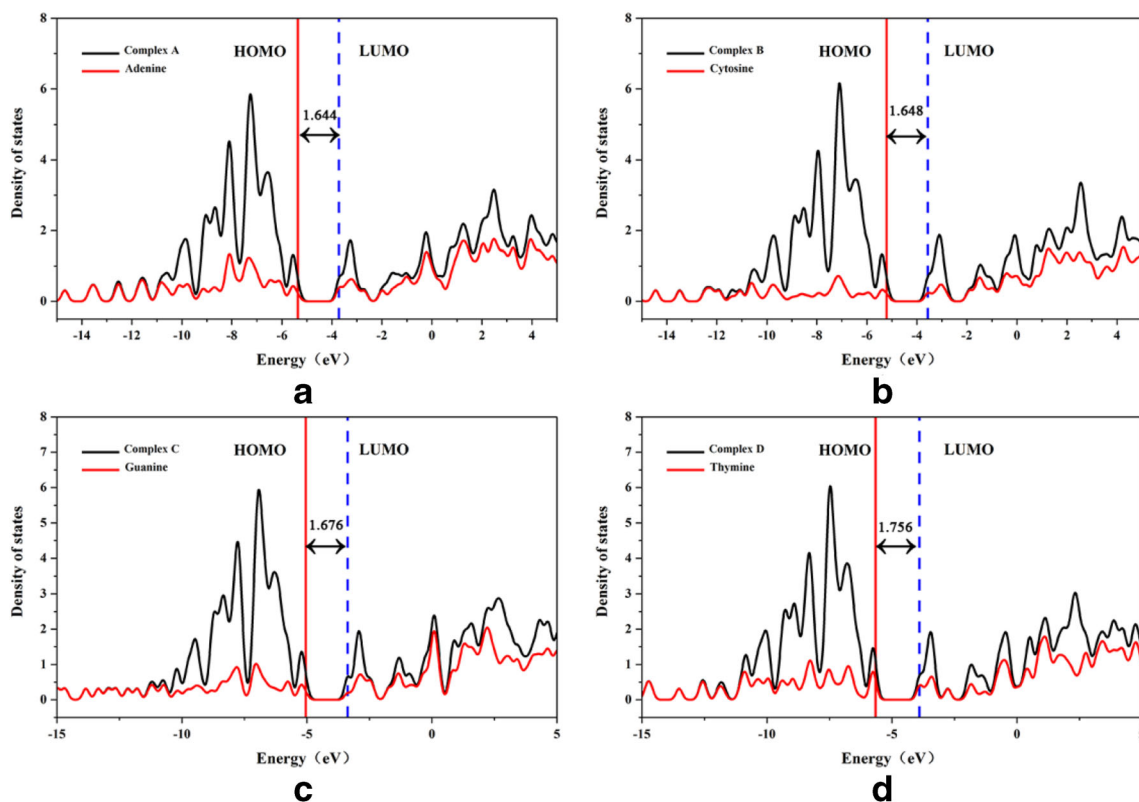


**Fig. 3** The total density of states (DOS) and partial DOS of nucleobase in different complexes, Au<sub>20</sub>/adenine (A), Au<sub>20</sub>/cytosine (B), Au<sub>20</sub>/guanine (C), and Au<sub>20</sub>/thymine (D)

QTAIM is one of the most powerful tools in modern theoretical chemistry [21]. The QTAIM provides a compact approach to cross advanced quantum chemistry and experimental approach [21–23], and unravels the interactions of molecules with the help of parameters, e.g., electron density  $\rho(r)$ , Laplacian of electron density  $\nabla^2\rho(r)$ , kinetic energy density ( $G$ ), and the potential energy density ( $V$ ). QTAIM parameters were obtained by using Multiwfn package [24]. In this study, natural bond orbital (NBO) analysis implemented in Gaussian 09 was also performed to reveal the interactions.

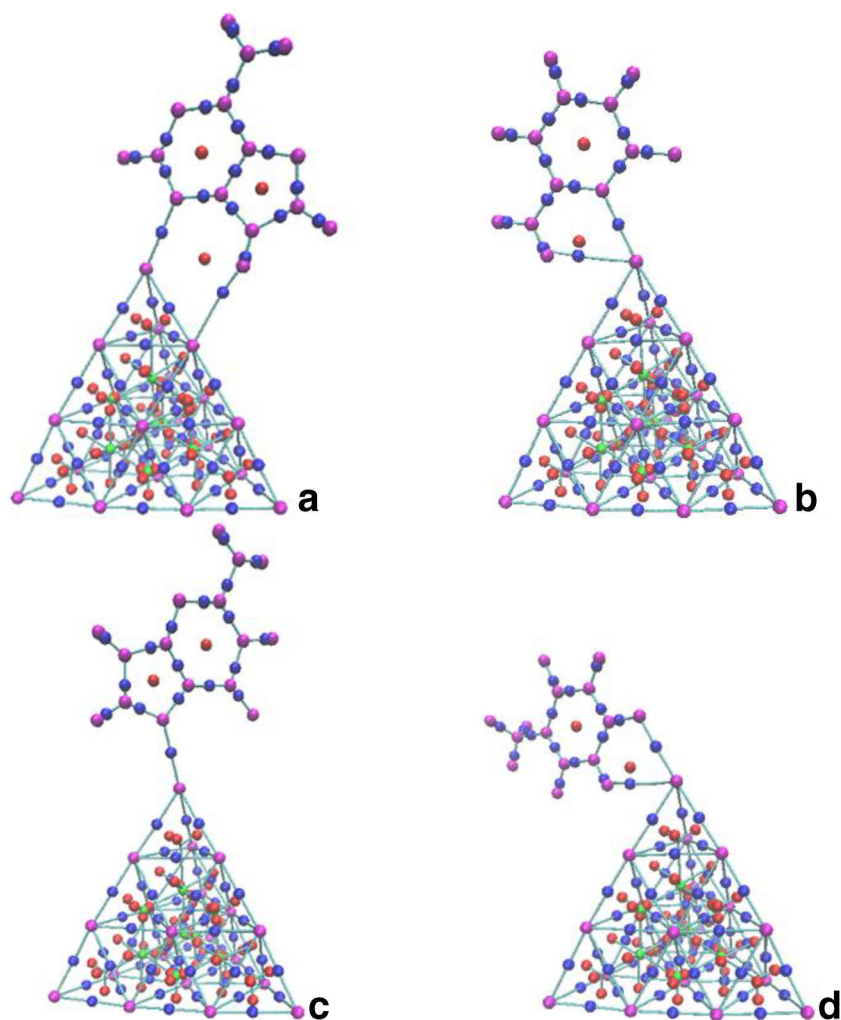
## Results and discussion

### Adsorption of nucleobases on Au<sub>20</sub> cluster

The Au<sub>20</sub> cluster is found to possess a pyramid structure which is a fragment of the face-centered cubic lattice of bulk gold. Three types of atoms corresponding to different coordination numbers are identified as A, B, and C shown in Fig. 1. The bond lengths of equilibrium geometries for the tetrahedral Au<sub>20</sub> cluster in our calculations are 2.86, 2.71, 2.76, 3.00, and 3.09 Å, respectively. The equilibrium bond lengths are very close to the results of Himadri De et al. [25].

The optimized structures of Au<sub>20</sub> with adenine (complex A) are shown in Fig. 2. The atom N31 is found to be

**Fig. 4** The molecular graph of  $Au_{20}$ /nucleobase complexes (A, B, C, and D are  $Au_{20}$ /adenine,  $Au_{20}$ /cytosine,  $Au_{20}$ /guanine, and  $Au_{20}$ /thymine, respectively). Blue spheres are bond critical points (purple, red and green spheres are nuclear attractor critical points, ring critical points, and cage critical points, respectively)



more preferable than the N9 to be adsorbed on the top site of  $Au_{20}$  corresponding to the Au–N bond length of 2.24 Å. Similarly, the atom N in cytosine tends to bond with Au atom in  $Au_{20}$ /cytosine (complex B) and  $Au_{20}$ -guanine (complex C); the distances of Au–N bonds are 2.25 Å in complex B and 2.24 Å in complex C, respectively. On the other hand, the O atom in thymine is bonded to Au atom in the complex D ( $Au_{20}$  with thymine) which corresponds to Au–O bond of 2.41 Å. The adsorption energies of the studied complexes were evaluated with basis set superposition error (BSSE) consideration.

As shown in Table 1, the orders of calculated adsorption energy are  $Au_{20}$ /cytosine (B) (–0.787 eV) >  $Au_{20}$ /adenine (A) (–0.690 eV) >  $Au_{20}$ /guanine (C) (–0.688 eV) >  $Au_{20}$ /thymine (D) (–0.328 eV). The maximum adsorption energy is –0.787 eV which belongs to the adsorption of cytosine. When considering the solvent effect, the adsorption energy decreased significantly in aqueous phase, but the adsorption strength order remains the same as that in the gas phase. From Table 1, one can find that the HOMO-LUMO gaps of  $Au_{20}$  were decreased upon the adsorption of nucleobases. The order of HOMO-LUMO

**Table 2** Topological parameters (in atomic units) for the optimized complexes

complex	interaction	$\rho$	$\nabla^2\rho$	G(r)	V(r)	$-V(r)/G(r)$	H(r)
A	Au...N	0.078	0.280	0.086	–0.103	1.198	–0.017
B	Au...N	0.077	0.272	0.084	–0.101	1.202	–0.017
C	Au...N	0.077	0.285	0.087	–0.103	1.184	–0.016
D	Au...O	0.048	0.191	0.052	–0.057	0.912	–0.005



**Table 3** NPA atomic charges (au) for complexes and Mayer bond order

Complex	Charge Au	Charge N	Charge O	Mayer
A	0.121	-0.606	-	0.876
B	0.142	-0.659	-	0.669
C	0.133	-0.542	-	0.842
D	0.072	-	-0.653	0.436

gap is D (1.756 eV) > C (1.676 eV) > B (1.648 eV) > A (1.644 eV). By comparing with free Au<sub>20</sub> cluster, the decreases in energy gaps ( $\Delta E_g$ ) were more than 10% for complexes, A, B, and C, suggesting the significant influence of nucleobases adsorption on electronic structure of Au<sub>20</sub>. The total density of states (DOS) of the studied complexes and the partial DOS of adsorbed nucleobase are depicted in Fig. 3. It is found that the DOS plots are significantly affected by the adsorption of nucleobase because the adsorbed nucleobases have a certain contribution to the total DOS near the HOMO/LUMO energy level. These results indicate that the electric conductivity of Au<sub>20</sub> cluster is sensitive for the nucleobase.

### Interaction characteristics

QTAIM theory provides a simple and efficient way to divide any system into fragments for ascertaining and visualizing the interaction of complexes. The molecular graphs of all studied complexes are illustrated in Fig. 4, and the topological parameters were listed in Table 2. All complexes have a positive  $\nabla^2\rho$  value, suggesting the closed-shell characteristics. However, we also note that  $H(r)$  values are negative, which indicates that their interactions show partial covalent [26]. According to Bader's theory, the property of natural interactions of the states showed as follows: when  $|V| < G$ , the property of bond is electrostatic; when  $|V| > G$ , the property of bond is covalent; and when  $G < |V| < 2G$ , the property of bond is partially covalent [27]. The  $-V/G$  values are 1.198, 1.202, and 1.184 for complexes A, B, and C, respectively, confirming the partial covalent character of these Au–N bonds in these complexes. On the other hand, the Au–O bond in complexes D shows

**Table 4** Most important acceptor-donor second-order perturbation energies ( $E^2$ ) for the interaction of Au<sub>20</sub> with nucleobases

Complex	Donor	Acceptor	$E^2$ (Kcal/mol)
A	LP (Au)	BD*(C–N)	2.94
B	LP (Au)	BD*(C–N)	2.49
C	LP (Au)	BD*(C–N)	2.99
D	LP (Au)	BD*(C–O)	1.41

(LP lone pair, BD double center bond)

electrostatic characteristic with a  $-V/G$  value (0.912) lower than 1. Moreover, electron density  $\rho$  also reflects the strength of the interaction, Au–O bond in complex D corresponds to a lower  $\rho$  value (0.048) relative to those of Au–N bonds in other complexes (either 0.077 or 0.078) as shown in Table 2. Therefore, the interaction between Au and O in complex D is weaker than Au–N bond in other complexes, which is in agreement with the results of adsorption energy.

NBO analysis is a high accuracy method for quantitative estimation of donor-acceptor interactions between complexes. As shown in Table 3, the Mayer bond order values of Au–N bonds in complexes A, B, and C are in the range of 0.669–0.876, suggesting a single-bond character. The Au–O bond in complexes D is weaker than the Au–N bonds revealed by the lower bond order (0.436). The natural population analysis (NPA) charges of the bonding atoms are shown in Table 3. As expected, due to the huge electronegativity of the N (O) atom in nucleobases, the charge transfers have occurred from Au<sub>20</sub> to nucleobases. We also note that the charge transfers from Au atom to N atom in complexes A, B, and C are slightly larger than that from Au atom to O atom in complex D, again confirming the stronger interaction between Au and N relative to Au–O interaction. The second-order perturbation energy ( $E^2$ ) of donor-acceptor interactions is provided in Table 4. The electrons were transferred from the lone pair of the bonding Au atom LP (Au) to the double center anti-bonding orbital of C–N in the A, B, and C complexes with  $E^2$  values in the range of 2.49–2.99 Kcal/mol. The  $E^2$  value relevant to Au–O interaction in complex D (Au<sub>20</sub>/thymine) is 1.41 Kcal/mol, which is significantly lower than other complexes; this indicates the weak interaction between Au<sub>20</sub> and thymine.

### IR spectra

The infrared spectra were simulated through frequency calculations. Figure 5 shows the IR spectra of the studied complexes at a full range of frequencies, and normal modes of the prominent IR active peaks in Fig. 5 are shown in Fig.S1. It can be seen that all absorption peaks are concentrated in two frequency bands, which are around 1630 cm<sup>-1</sup> and 3350 cm<sup>-1</sup>, respectively. These two features were also identified in Zwitterion L-cysteine (Z-cys) adsorbed Au<sub>20</sub> cluster [28]. In the previous report, the frequency of NH<sub>2</sub> scissors mode has been confirmed as 1607 cm<sup>-1</sup>, and the C=O stretching mode and N–H stretching mode are located at 1628 cm<sup>-1</sup> and 3026 cm<sup>-1</sup>, respectively. For complex A, the adsorption peak at 1629 cm<sup>-1</sup> is mainly from the NH<sub>2</sub> scissors mode, and adsorption peak at 3365 cm<sup>-1</sup> from the N–H stretching. It is obvious that the N–H stretching frequency in complex A is about 300 cm<sup>-1</sup> higher than that in Z-cys/Au<sub>20</sub> species. The complex B shows the predominant absorption peak at 3354 cm<sup>-1</sup> corresponding to the N–H stretching instead of around 1630 cm<sup>-1</sup>. The C=O stretching vibration at

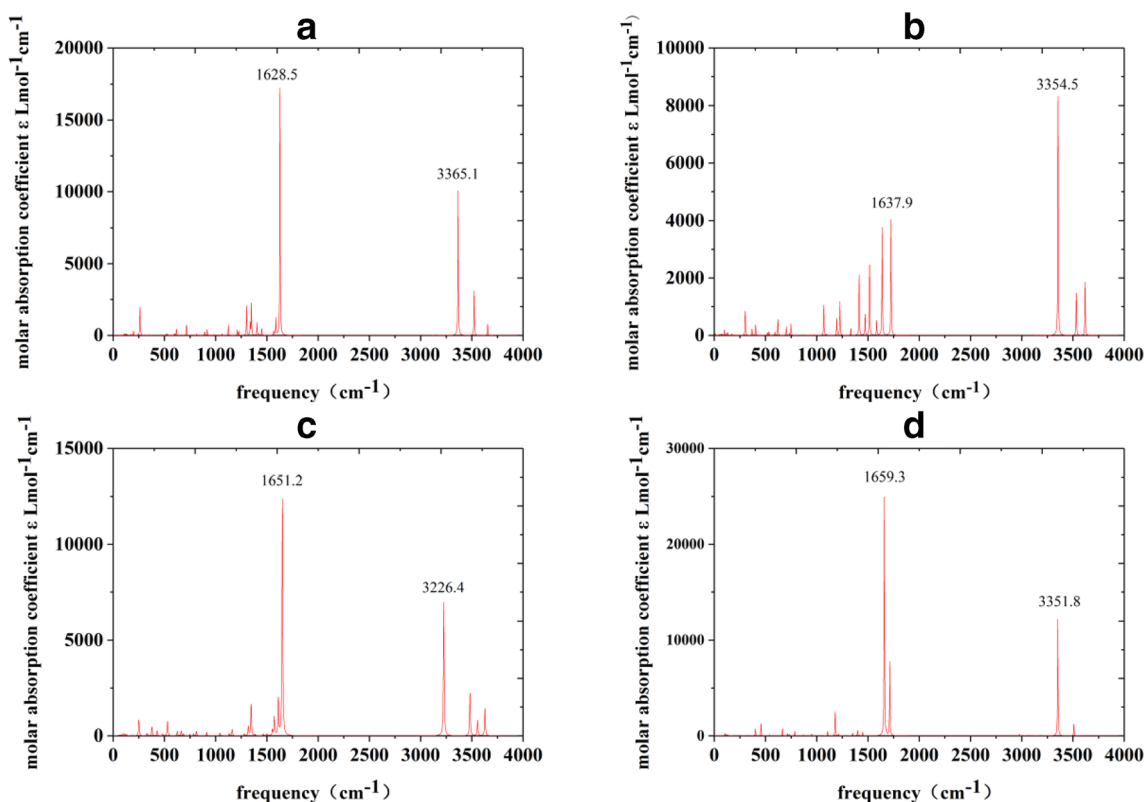


**Fig. 5** Simulated IR spectra for (A) complex A, (B) complex B, (C) complex C, (D) complex D

1630  $\text{cm}^{-1}$  in complex B is very close to that in Z-cys/Au<sub>20</sub> complex (1628  $\text{cm}^{-1}$ ). The maximum IR peak of compounds C and D is also near 1630  $\text{cm}^{-1}$ . For complex C, the NH<sub>2</sub> scissors mode is dominant, and for complex D, it is C=O stretching vibration. For the second absorption peak around 3350  $\text{cm}^{-1}$ , it is from the symmetric stretching vibration of N–H in the NH<sub>2</sub> group in complex C, and from the N–H stretching in complex D. Through analyzing the fingerprint region of the spectrum, we found that the vibrations relevant to the metal atoms in Au<sub>20</sub> cluster only appear in the low frequency regions lower than 200  $\text{cm}^{-1}$  in the infrared spectrum.

## UV-vis spectra

UV-vis spectra of the studied complexes have been obtained with time-dependent density-functional theory (TDDFT) calculations at PBE level of theory with 60 states considered. The simulated UV-vis spectra of free Au<sub>20</sub> and complexes were shown in Fig. S2 and Fig. 6, respectively. As shown in Fig. S2, two appearance peaks at 478 nm and 607 nm (see Table 5) emerged in UV-vis spectra of free Au<sub>20</sub> cluster. We can make a preliminary judgment of transition orbitals through the isosurface change of different orbitals. One can see from Fig. S3 that both peaks in UV-vis spectra of Au<sub>20</sub> are regarded as the transition from Au(d) → Au

**Table 5** Excitation, wavelengths  $\lambda$  (nm), oscillator strengths  $f$ , maximum transitions, and excitation coefficients (%) for free Au<sub>20</sub> cluster and complexes

Complex	Excitation	$\lambda$	$f$	Maximum transition	Excitation coefficients
Au <sub>20</sub>	S <sub>0</sub> → S <sub>57</sub>	478	0.017	H → L + 9	23.6
	S <sub>0</sub> → S <sub>14</sub>	607	0.026	H-3 → L + 1	41.3
A	S <sub>0</sub> → S <sub>53</sub>	484	0.043	H-9 → L + 1	32.9
	S <sub>0</sub> → S <sub>12</sub>	613	0.017	H-4 → L	34.3
B	S <sub>0</sub> → S <sub>59</sub>	484	0.013	H-9 → L + 1	36.9
	S <sub>0</sub> → S <sub>10</sub>	633	0.015	H-3 → L	29.6
C	S <sub>0</sub> → S <sub>56</sub>	483	0.042	H-9 → L + 1	46.7
	S <sub>0</sub> → S <sub>9</sub>	631	0.014	H-3 → L + 1	35.4
D	S <sub>0</sub> → S <sub>55</sub>	485	0.030	H-9 → L	25.7
	S <sub>0</sub> → S <sub>9</sub>	626	0.014	H-3 → L + 1	27.4

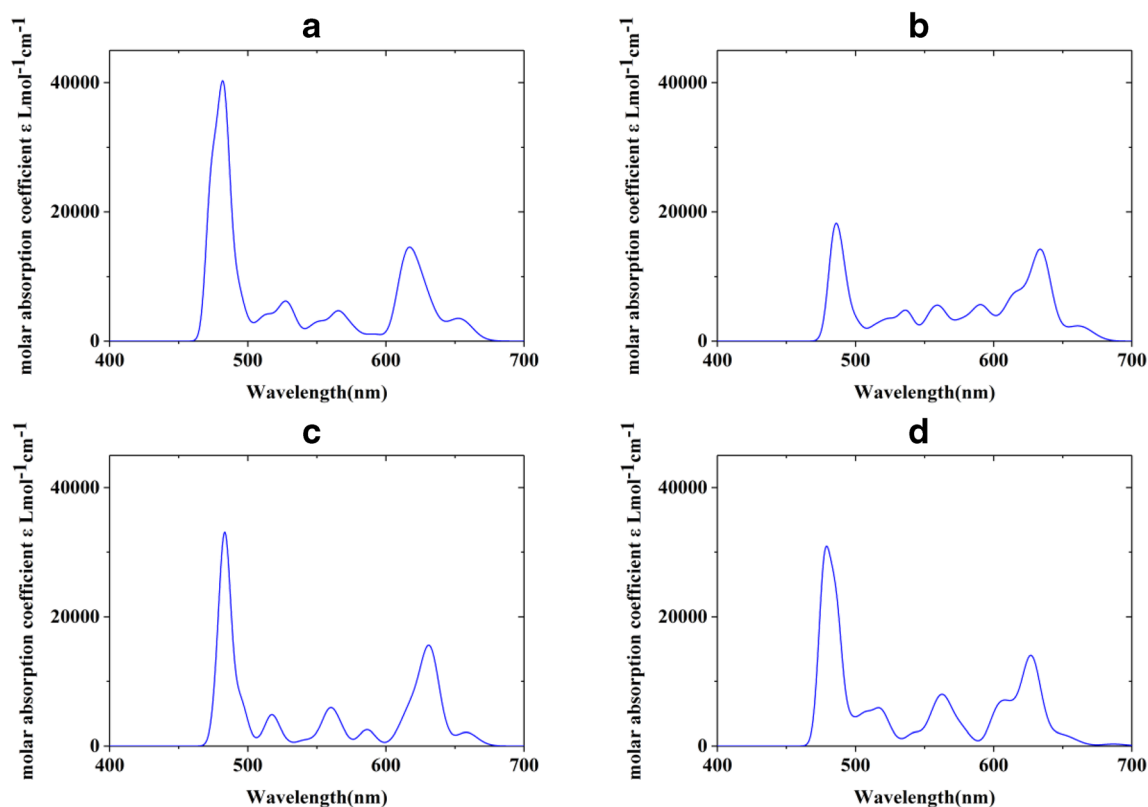


**Fig. 6** Simulated UV-vis spectra for (A) complex A, (B) complex B, (C) complex C, (D) complex D

(s). As shown in Fig. 6, there are also two dominating peaks in the UV-vis spectra of the studied complexes. We also note that the peaks of complexes show a certain amount of redshift compared to free  $Au_{20}$  cluster due to the adsorption of nucleobases. As shown in Table 5, the predominant peak at 484 nm in complex A (see Fig. 6) is identified as the transition from the H-9 to L + 1 orbitals, and the second peak at 613 nm is from H-4 to L. The first peak transition is from Au (p)  $\rightarrow$  Au (d), and the second peak transition is from Au (p)  $\rightarrow$  Au (s). For complex B, the dominant transition is from H-9 to L + 1 for the peak at 484 nm, the dominant transition for the second peak at 633 nm is from orbital H-3 to L, and the transition types of these peaks are Au (s)  $\rightarrow$  Au (p) and Au (d)  $\rightarrow$  Au (p), respectively. Complex C show dominating peaks at 483 nm and 631 nm, respectively, and the transition types are both Au (d)  $\rightarrow$  Au (p). The peak at 485 nm for complex D is from orbital H-9 to L, corresponding to Au (d)  $\rightarrow$  Au (p) transition, and the other obvious peak at 626 nm is from orbital H-3 to L + 1. On the whole, the main peaks in the UV-vis spectra of studied complexes are mainly attributed from the metal-to-metal charge transfers.

## Conclusions

In our research, the adsorption of nucleobases on  $Au_{20}$  cluster was investigated by density functional theory.

We find that the gold atoms are more tend to interact with the nitrogen atom in the base group than with the oxygen atom. The orders of adsorption strength are  $Au_{20}$ /cytosine (B) ( $-0.787$  eV)  $>$   $Au_{20}$ /adenine (A) ( $-0.690$  eV)  $>$   $Au_{20}$ /guanine (C) ( $-0.688$  eV)  $>$   $Au_{20}$ /thymine (D) ( $-0.328$  eV). Upon the adsorption of nucleobases, the energy gaps of  $Au_{20}$  were significantly decreased relative to the isolated one. The results of QTAIM indicated the  $Au_{20}$  bonds to adenine, cytosine, guanine with partial covalent interaction; the interaction between  $Au_{20}$  and thymine was main electrostatic nature. NBO analysis indicated that the electrons were transferred from the lone pair of the Au atom to the anti-bonding orbital of the C–N or C–O. The considerable charge transfers from  $Au_{20}$  to nucleobases account for the strong interaction. In summary, the moderate adsorption energies, considerable charge transfer, and significant energy gap changes indicate that the  $Au_{20}$  cluster is feasible as a promising sensor for nucleobases. Moreover, we simulated the IR and UV-vis spectrum to provide a theoretical reference for further experiment.

**Supplementary Information** The online version contains supplementary material available at <https://doi.org/10.1007/s00894-020-04618-8>.

**Funding** This work is supported by the Project of Education Department in Sichuan Province (No. 15ZB0006).

## References

- Stepanian SG (2014) Interactions of the Watson–Crick nucleic acid base pairs with carbon nanotubes and graphene: DFT and MP2 study. *Chem Phys Lett* 610:186–191
- Odenthal KJ, Gooding JJ (2007) An introduction to electrochemical DNA biosensors. *ANALYST* 132(7):603–610
- Gowtham S, Scheicher RH, Pandey R (2008) First-principles study of physisorption of nucleic acid bases on small-diameter carbon nanotubes. *NANOTECHNOLOGY* 19(12):125701
- Kim JH, Kataoka M, Jung YC (2013) Mechanically tough, electrically conductive polyethylene oxide nanofiber web incorporating DNA-wrapped double-walled carbon nanotubes. *ACS Appl Mater Inter* 5(10):4150–4154
- Johnson RR, Johnson ATC, Klein ML (2010) The nature of DNA-base-carbon-nanotube interactions. *Small Methods* 6(1):31–34
- Castañeda MT, Alegret S, Merkoçi A (2007) Electrochemical sensing of DNA using gold nanoparticles. *ELECTROANAL* 19(7–8):743–753
- Chen YS (2009) Assessment of the in vivo toxicity of gold nanoparticles. *Nanoscale Res Lett* 4(8):858–864
- Ceconello A (2013) Au nanoparticle/DNA rotaxane hybrid nanostructures exhibiting switchable fluorescence properties. *Nano Lett* 13(12):6275–6280
- Li J (2003) Au<sub>20</sub>: a tetrahedral cluster. *Science* 299(5608):864–867
- Yuan Y, Cheng L, Yang J (2013) Electronic stability of phosphine-protected Au<sub>20</sub> nanocluster: superatomic bonding. *J Phys Chem C* 117(25):13276–13282
- Wan XK, Lin ZW, Wang QM (2012) Au<sub>20</sub> nanocluster protected by hemilabile phosphines. *J Am Chem Soc* 134(36):14750–14752
- Munoz-Castro A, King RB (2017) Au-20. Effect of a strong tetrahedral field in a spherical concentric bonding shell model. *J Phys Chem C* 121(10):5848–5853
- Yu CQ (2017) Intense fluorescence of Au-20. *J Phys Chem C* 147(9)
- Guo JH (2014) Enhanced fluorescence from dye molecules by Au nanoparticles on asymmetric double-stranded DNA and mechanism. *Appl Phys Lett* 104(14):141910
- Hull JM, Provorse MR, Aikens CM (2012) Formylxyl radical–gold nanoparticle binding: a theoretical study. *J Phys Chem A* 116(22):5445–5452
- Joshi K, Krishnamurthy S (2015) Behaviour of ‘free-standing’ hollow Au nanocages at finite temperatures: a BOMD study. *Mol Phys* 113(19–20):2980–2991
- Love PED, Teo P (2017) Statistical analysis of injury and nonconformance frequencies in construction: negative binomial regression model. *J Constr Eng Manag* 143(8):05017011
- Frisch MJ, Trucks GW, Schlegel HB (2009) Gaussian 09, Revision A.02. Gaussian, Inc., Wallingford CT
- Raghavachari K (2000) Perspective on “density functional thermochemistry. III. The role of exact exchange”. *Theor Chem Accounts* 103(3–4):361–363
- Hurtado RB (2017) Random alloy of Au–Ag bimetallic nanoparticles at room temperature-facile synthesis and vibrational properties. *Gold Bull* 2:85–92
- Ravaei I, Haghighat M, Azami SM (2019) A DFT, AIM and NBO study of isoniazid drug delivery by MgO nanocage. *Appl Surf Sci* 469:103–112
- Nemati-Kande E, Abbasi M, Mohammadi MD (2019) Feasibility of pristine and decorated AlN and SiC nanotubes in sensing of noble gases: a DFT study. *ChemistrySelect* 4(8):2453–2462
- Ribeiro I, Reis D, Pereira D (2019) A DFT-based analysis of adsorption of Cd<sup>2+</sup>, Cr<sup>3+</sup>, Cu<sup>2+</sup>, Hg<sup>2+</sup>, Pb<sup>2+</sup>, and Zn<sup>2+</sup>, on vanillin monomer: a study of the removal of metal ions from effluents. *J Mol Model* 25(9):267
- Lu T, Chen FW (2012) Multiwfn: a multifunctional wavefunction analyzer. *J Comput Chem* 33(5):580–592
- De H, Paul A, Datta A (2017) Theoretical study of Au<sub>4</sub> thymine, Au<sub>20</sub> and Ag<sub>20</sub> uracil and thymine complexes for surface enhanced Raman scattering. *Comput Theor Chem* 1111:1–13
- Cemer D, Kraka E (1984) Chemical bonds without bonding electron density does the difference electron-density analysis suffice for a description of the chemical bond? *Angew Chem Int Edit* 23(8):617
- Espinosa E, Alkorta I, Elguero J, Molins E (2002) From weak to strong interactions: a comprehensive analysis of the topological and energetic properties of the electron density distribution involving X–HF–Y systems. *J Chem Phys* 117:5529
- Tlahuice-Flores A (2013) Zwitterion l-cysteine adsorbed on the Au<sub>20</sub> cluster: enhancement of infrared active normal modes. *J Mol Model* 19:1937–1942

**Publisher's note** Springer Nature remains neutral with regard to jurisdictional claims in published maps and institutional affiliations.